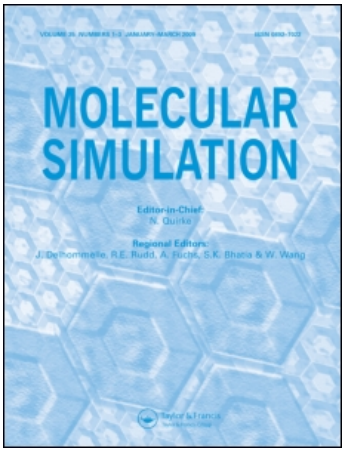

Molecular Simulation
Publication details, including instructions for authors and subscription information:
http://www.informaworld.com/smpp/title~content=t713644482

Molecular dynamics simulation of reorientation of polyethylene chains under a high magnetic field

M. S. Al-Haik[a]; M. Y. Hussaini[b]
[a] Department of Mechanical Engineering, University of NewMexico, Albuquerque, NM, USA [b] School of Computational Science, Florida State University, Tallahassee, FL, USA

To cite this Article Al-Haik, M. S. and Hussaini, M. Y.(2006) 'Molecular dynamics simulation of reorientation of polyethylene chains under a high magnetic field', Molecular Simulation, 32: 8, 601 — 608
To link to this Article: DOI: 10.1080/08927020600887781
URL: http://dx.doi.org/10.1080/08927020600887781

Molecular Simulation, Vol. 32, No. 8, 15 July 2006, 601–608

Taylor & Francis
Taylor & Francis Group

Molecular dynamics simulation of reorientation of polyethylene chains under a high magnetic field

M. S. AL-HAIK†* and M. Y. HUSSAINI‡

†Department of Mechanical Engineering, University of NewMexico, Albuquerque, NM 87131, USA
‡School of Computational Science, Florida State University, Tallahassee, FL 32306, USA

(Received May 2006; in final form June 2006)

The purpose of this investigation is to clarify the dynamical process of reorientation of a polyethylene chains under high magnetic fields. Molecular dynamics (MD) simulations at constant temperature and pressure are carried out to study the reorientation of two polyethylene chains with different configurations. We utilized static homogeneous external magnetic fields of 25 T into the velocity Verlet integration algorithm through a suitable Taylor expansion.

Simulations reveal that the gained potential energy through magnetic annealing facilitated the reorganization of the polyethylene chains closer to the direction of the applied magnetic field. The current study offer an alternative explanation for the orientation that was not available through the hydrodynamics continuum approach based on the diamagnetic susceptibilities as the driving force for reorientation.

Keywords: High magnetic field; Velocity Verlet; OPLSAA force field; Polymer

1. Introduction

The physical and mechanical properties of polymers strongly depend on their degree of orientational order. The ongoing quest for designing and synthesizing novel molecular materials, understanding their intrinsic properties and improving their performance in real devices, therefore requires full control over their spatial arrangement.

Modern chemistry often uses self-organization of molecular building blocks [1], making use of liquid crystallinity or self-assembly of anisotropic molecules, to form architectures that are well defined on a nano- or micro-scopic length scale. One of the major remaining challenges is to induce orientational order extending to a macroscopic level [2], either by directly programming the molecular units to do so (supramolecular chemistry) or by aligning the material by other means, such as stretching [3], streaming or application of external electric [4] or magnetic fields [5].

Magnetic field induced-alignment of polymeric materials has been the focus of several research efforts [5–8]. Polymeric materials can interact with a magnetic field through the diamagnetic anisotropy of the constituent chemical units. The energy that the chemical unit gains through the interaction with an external magnetic field is dependent on the orientation of the unit relative to the magnetic field and hence the unit tends to align in a direction that would minimize its energy [8]. The tendency of a unit to align is suppressed by the thermal agitation, if the energy reduction due to alignment cannot compensate the energetic penalty that arises due to the expenditure of thermal energy. This is the case for non-liquid crystalline polymers in melts and solutions. The application of a magnetic field has a significant effect on the orientation of liquid-crystalline materials through the interaction with molecules with diamagnetic anisotropy. Polymer molecules tend to align with their chain axes parallel to a magnetic field, especially when the randomizing effect of thermal energy is reduced by the orientation of the molecules within a mesophase [9].

In a magnetic field B, a diamagnetic molecule acquires an extra energy $E = -\Delta\chi B^2$, where χ is the molecular diamagnetic susceptibility. In general, $\Delta\chi$ is the anisotropic diamagnetic susceptibility, expressed by $\Delta\chi = \chi_{\parallel} - \chi^{\perp}$ the difference in susceptibility along two orthogonal molecular axes.

*Corresponding author. Email: alhaik@unm.edu

Molecular Simulation
ISSN 0892-7022 print/ISSN 1029-0435 online © 2006 Taylor & Francis
http://www.tandf.co.uk/journals
DOI: 10.1080/08927020600887781

For individual molecules, the change in energy is small compared to the thermal energy ($\Delta\chi B^2 << kT$) and it is not possible to magnetically align single molecules at fields that are experimentally accessible nowadays. Magnetic orientation is therefore only applicable to materials such as macromolecules (polymers), liquid crystals or molecular aggregates, that contain a sufficient amount of coupled or correlated molecules (N) to result in a magnetic torque that is large enough to induce appreciable orientational order ($N\Delta\chi B^2 > kT$) [2]. For a polymer chain with N moles to rotate by an angle θ (angle between the magnetic field and the tube-axis) in a magnetic field with intensity B inside a medium with viscosity η, then the following condition should be satisfied [10]

$$-B^2N(\chi_\perp \cos^2\theta + \chi_\parallel \sin^2\theta) > k_b T + \frac{8\pi\eta a^3 D}{F(D)} \qquad (1)$$

where k_b is the Boltzmann's constant, T is the temperature in Kelvin, a is the characteristic length, D is the aspect ratio and $F(D)$ is a front factor (function of the aspect ratio). However, in previous investigations of the alignment of isotactic polystyrene [11], it was stated that the viscosity is too high to explain the observed rate of alignment in terms of the rotation mechanism given by equation (1). Similarly, the authors were able to align commercial highly-viscous epoxy (Aerpoxy™) under magnetic fields of 15–25 T and quantify these alignments through X-ray diffraction and microscopy analysis [5,12,13]. The rotation model was incapable of explaining the alignment of the Aerpoxy under 25 T field as the high viscosity of the Aeropoxy (95 N/s/m^2) will generate high drag force that prohibits the rotation and alignment of the epoxy.

The purpose of this investigation is to clarify the dynamical process of reorientation of a polyethylene chains under high magnetic fields. To this end, we perform molecular dynamics (MD) simulations for the polyethylene chain with two different initial configurations (heavily-folded and helical chains) to study the polymer chain unfolding and reorientation process under high magnetic field. We believe that such simulations enhance our understanding of the molecular motion leading to the alignment of polymeric materials to produce high-performance materials.

2. Molecular dynamics at strong external magnetic field

The idea of introducing an external force field in the MD simulations of polymeric materials is relatively recent. Weber and Annan [14] conducted an adiabatic MD simulation of ethane molecules under the influence of external compression and shearing forces. Strong external fields were found to align the molecules in the direction of the shearing field. Tian *et al.* [15] performed MD simulation study of the switching dynamics of nematics liquid crystals with positive polarity anisotropy under an applied electric field with different strengths and observed unidirectional switching.

Considering a system of N particle, MD is the problem of solving numerically Newton's equation of motion for the system of many particles interacting with each other

$$F_i = m_i \frac{d^2 r_i}{dt^2} = -\partial \frac{E(r_1, r_2, \ldots, r_N)}{\partial r_i} \qquad (2)$$

where m_i is the atomic mass of the i-th atom, RI is the atom position relative to a reference coordinates and E the potential energy of the system. Successive configurations of the system are generated by the time integration of equation (2). The result is a trajectory that specifies how the positions and velocities of the particles in the system vary with time

In the present study, we represent a system of a single polyethylene chain as a system of charged particles exposed to external static homogeneous magnetic field. The explicit time-stepping in a conventional MD simulation of such a system is restricted by the smaller of the two time scales—Larmor time-scale and characteristic time of the internal interactions of the system. In a high magnetic field, which is the context of the present study, the Larmor time-scale is very much smaller than that of the internal interactions and therefore the MD simulation becomes prohibitively expensive. Hence, we employ the algorithm due to Spreiter and Walter [16], which relaxes the Larmor restriction while maintaining the overall accuracy of the discretization scheme.

Under the influence of a continuous potential the motions of all particles are coupled together, giving rise to many-body problem that can not be solved analytically. Under such circumstances the equations of motion are integrated using finite difference method.

The velocity Verlet time-integration method [17] gives the positions, velocities and accelerations of the particles.

$$\begin{aligned}
\vec{r}(t+\delta t) &= \vec{r}(t) + \delta t\vec{v}(t) + \frac{1}{2}(\delta t)^2\vec{a}(t) + O((\delta t)^3) \\
\vec{a}(t+\delta t) &= \vec{a}(\vec{r}_1(t+\delta t), \ldots, \vec{r}_N(t+\delta t); \\
&\qquad \vec{v}_1(t+\delta t), \ldots, \vec{v}_N(t+\delta t); t+\delta t) \\
\vec{v}(t+\delta t) &= \vec{v}(t) + \delta t\vec{v}(t) + \frac{1}{2}\delta t[\vec{a}(t) + \vec{a}(t+\delta t)] + O((\delta t)^3)
\end{aligned} \qquad (3)$$

A particle with specific charge q_i/m_i performs Larmor oscillations of frequency $\omega_i = q_i B/m_i$ when influenced by a magnetic field B. With a homogeneous magnetic field $\mathbf{B} = (0, 0, B)$ along the z-axis, the acceleration of each particle is given by:

$$\vec{a}_i(t) = \vec{a}_i^C(t) - \omega\vec{e}_z \times \vec{v}_i(t) \qquad (4)$$

where $a_i^c(t)$ is the part of acceleration which does not depend on velocities; $a_i^c(t) = a^{\mathrm{C}}(r_{1i}(t), \ldots, r_{Ni}(t); t)$, e_z is the unit vector along the z direction.

Assuming the magnetic field strong such that $\omega\delta t = O((\delta t)^0)$, utilizing Taylor series expansion for $(\vec{r}(t+\Delta t)$ and $\vec{v}(t+\Delta t)$

$$\vec{r}(t+\delta t) = \vec{r}(t) + \delta t\vec{v}(t) + \sum_{n=2}^{\infty} \frac{(\delta t)^n \mathrm{d}^{n-2}}{n!} \frac{\mathrm{d}^{n-2}}{\mathrm{d}t^{n-2}} \vec{a}(t) \quad (5)$$

$$\vec{v}(t+\delta t) = \vec{v}(t) + \delta t\vec{a}(t) + \sum_{n=2}^{\infty} \frac{(\delta t)^n \mathrm{d}^{n-2}}{n!} \frac{\mathrm{d}^{n-1}}{\mathrm{d}t^{n-1}} \vec{a}(t) \quad (6)$$

Utilizing equation (4) and $\vec{a} = \mathrm{d}\vec{v}/\mathrm{d}t$

$$\begin{aligned} \frac{\mathrm{d}^{n-2}}{\mathrm{d}t^{n-2}}\vec{a} &= \frac{\mathrm{d}^{n-2}}{\mathrm{d}t^{n-2}}\vec{a}^{\,c} - \omega\vec{e}_z \times \frac{\mathrm{d}^{n-2}}{\mathrm{d}t^{n-2}}\vec{v} \\ &= \frac{\mathrm{d}^{n-2}}{\mathrm{d}t^{n-2}}\vec{a}^{\,c} - \omega\vec{e}_z \times \frac{\mathrm{d}^{n-3}}{\mathrm{d}t^{n-3}}\vec{a} \end{aligned} \quad (7)$$

To deal with the cross product on the x and y components we utilize the complex mapping

$$\begin{aligned} &R^3 \rightarrow C; \quad \bar{n} \mapsto n = n_x + in_y \\ &C \rightarrow R^3; \quad \vec{n} \mapsto n = n_\alpha + in_\beta \mapsto \vec{n} = (n_\alpha, n_\beta, 0) \end{aligned} \quad (8)$$

The z component of the position is not affected by the magnetic field (since the magnetic field in the z direction) thus the cross product $\vec{e}_z \times \vec{a}$ can be mapped into a simple multiplication $\vec{e}_z \times \vec{a} \mapsto -a_y + ia_x = ia$. Substituting this result back in equation (7),

$$\frac{\mathrm{d}^{n-2}}{\mathrm{d}t^{n-2}}\vec{a} = \frac{\mathrm{d}^{n-2}}{\mathrm{d}t^{n-2}}\vec{a}^{\,c} - i\omega\frac{\mathrm{d}^{n-3}}{\mathrm{d}t^{n-3}}\vec{a}. \quad (9)$$

Putting equation (9) into itself $(n-3)$ times recursively and applying equation (4)

$$\begin{aligned} \frac{\mathrm{d}^{n-2}}{\mathrm{d}t^{n-2}}\vec{a} = \frac{\mathrm{d}^{n-2}}{\mathrm{d}t^{n-2}}\vec{a}^{\,c} - i\omega\Bigg\{ &\frac{\mathrm{d}^{n-3}}{\mathrm{d}t^{n-3}}\vec{a}^{\,c} \\ &- i\omega\left(\frac{\mathrm{d}^{n-4}}{\mathrm{d}t^{n-4}}\vec{a}^{\,c} \ldots - i\omega(\vec{a}^{\,c} - i\omega\vec{v})\right)\Bigg\} \end{aligned} \quad (10)$$

Collecting the highest terms of ω gives

$$\begin{aligned} \frac{\mathrm{d}^{n-2}}{\mathrm{d}t^{n-2}}\vec{a} &= (-i\omega)^{n-1}\vec{v} + (-i\omega)^{n-2}\vec{a}^{\,c} \\ &\quad + \sum_{k=1}^{n-2} (-i\omega)^{n-2-k} \frac{\mathrm{d}^k}{\mathrm{d}t^k}\vec{a}^{\,c} \\ &= (-i\omega)^{n-1}\vec{v} + (-i\omega)^{n-2}\vec{a}^{\,c} + O((\delta t)^{3-n}) \end{aligned} \quad (11)$$

Substituting back in the general term of the series expansion in equation (5)

$$\begin{aligned} \frac{(\delta t)^n \mathrm{d}^{n-2}}{n!} \frac{\mathrm{d}^{n-2}}{\mathrm{d}t^{n-2}}\vec{a} &= \frac{(-i\omega\delta t)^n}{n!}\left(\frac{\vec{v}}{-i\omega} + \frac{\vec{a}^{\,c}}{(-i\omega)^2}\right) \\ &\quad + O((\delta t)^3) \end{aligned} \quad (12)$$

Substituting equation (12) back in the original Taylor expansion in equation (5) leads to

$$\begin{aligned} \vec{r}(t+\delta t) &= \vec{r}(t) + \delta t\vec{v}(t) \\ &\quad + \sum_{n=2}^{\infty}\left[\frac{(-i\omega\delta t)^n}{n!}\left(\frac{\vec{v}}{-i\omega} + \frac{\vec{a}^{\,c}}{(-i\omega)^2}\right) + O((\delta t)^3)\right] \\ &= \vec{r}(t) + \delta t\vec{v}(t) + [\exp(-i\omega\delta t) - 1 - i\omega\delta t] \\ &\quad \times \left(\frac{\vec{v}}{-i\omega} + \frac{\vec{a}^{\,c}}{(-i\omega)^2}\right) + O((\delta t)^3) \end{aligned} \quad (13)$$

Applying the inverse mapping $C \rightarrow R^3$ (equation (8)) to obtain the x and y components, while the z component remains unchanged

$$\begin{aligned} r_x(t+\delta t) &= r_x(t) + \frac{1}{\omega}[v_x(t)\sin(\omega\delta t) - v_y(t)C(\omega\delta t)] \\ &\quad + \frac{1}{\omega^2}\left[-a_x^c(t)C(\omega\delta t) - a_y^c(t)S(\omega\delta t)\right] + O((\delta t)^3) \\ r_y(t+\delta t) &= \text{like } r_x(t+\delta t), \text{exchange } x \leftrightarrow y, \quad \omega \leftrightarrow -\omega \\ r_z(t+\delta t) &= r_z(t) + \delta t v_z(t) + \frac{1}{2}(\delta t)^2 a_z^c(t) + O((\delta t)^3) \end{aligned} \quad (14)$$

where $S(\omega\delta t) = \sin(\omega\delta t) - \omega\delta t$, $C(\omega\delta t) = \cos(\omega\delta t) - 1$.

For the velocity replacing n by $n+1$ in equation (9),

$$\frac{\mathrm{d}^{n-1}}{\mathrm{d}t^{n-1}}\vec{a} = \frac{\mathrm{d}^{n-1}}{\mathrm{d}t^{n-1}}\vec{a}^{\,c} - i\omega\frac{\mathrm{d}^{n-2}}{\mathrm{d}t^{n-2}}\vec{a} \quad (15)$$

Which can be put into itself $(n-1)$ times, recursively, to yield

$$\begin{aligned} \frac{\mathrm{d}^{n-1}}{\mathrm{d}t^{n-1}}\vec{a} = \frac{\mathrm{d}^{n-1}}{\mathrm{d}t^{n-1}}\vec{a}^{\,c} - i\omega\Bigg\{ &\frac{\mathrm{d}^{n-2}}{\mathrm{d}t^{n-2}}\vec{a}^{\,c} - i\omega\Bigg(\frac{\mathrm{d}^{n-3}}{\mathrm{d}t^{n-3}}\vec{a}^{\,c} \ldots \\ &- i\omega(\vec{a}^{\,c} - i\omega\vec{v})\Bigg)\Bigg\} \end{aligned} \quad (16)$$

Collecting the highest orders of ω

$$\begin{aligned} \frac{\mathrm{d}^{n-1}}{\mathrm{d}t^{n-1}}\vec{a} &= (-i\omega)^n\vec{v} + (-i\omega)^{n-1}\vec{a}^{\,c} + (-i\omega)^{n-2} \\ &\quad \times \frac{\mathrm{d}}{\mathrm{d}t}\vec{a}^{\,c} + \sum_{k=2}^{n-1}(-i\omega)^{n-1-k}\frac{\mathrm{d}^k}{\mathrm{d}t^k}\vec{a}^{\,c} \\ &= (-i\omega)^n\vec{v} + (-i\omega)^{n-1}\vec{a}^{\,c} + (-i\omega)^{n-2} \\ &\quad \times \frac{\mathrm{d}}{\mathrm{d}t}\vec{a}^{\,c} + O((\delta t)^{3-n}) \end{aligned} \quad (17)$$

The general series term in equation (6) can now be rewritten using equation (17)

$$\begin{aligned} \frac{(\delta t)^n \mathrm{d}^{n-1}}{n!} \frac{\mathrm{d}^{n-1}}{\mathrm{d}t^{n-1}}\vec{a} &= \frac{(-i\omega\delta t)^n}{n!}\left(\vec{v} + \frac{\vec{a}^{\,c}}{-i\omega} + \frac{\mathrm{d}\vec{a}^{\,c}/\mathrm{d}t}{(-i\omega)^2}\right) \\ &\quad + O((\delta t)^3) \end{aligned} \quad (18)$$

Substituting back in equation (6) yields,

$$\vec{v}(t+\delta t) = \vec{v}(t) + \delta t[\vec{a}^{\,c}(t) - i\omega\vec{v}(t)] + \sum_{n=2}^{\infty}\left[\frac{(-i\omega\delta t)^n}{n!}\left(\vec{v}(t) + \frac{\vec{a}^{\,c}(t)}{(-i\omega)} + \frac{\mathrm{d}\vec{a}^{\,c}(t)/\mathrm{d}t}{(-i\omega)^2}\right) + O((\delta t)^3)\right] = \vec{v}(t) + \delta t[\vec{a}^{\,c}(t) - i\omega\vec{v}(t)] + [\exp(-i\omega\delta t) - 1 + i\omega\delta t] \times \left(\vec{v}(t) + \frac{\vec{a}^{\,c}(t)}{(-i\omega)} + \frac{\mathrm{d}\vec{a}^{\,c}(t)/\mathrm{d}t}{(-i\omega)^2}\right) + O((\delta t)^3) \tag{19}$$

Applying the inverse complex mapping to obtain the x and y components of the velocity

$$v_x(t+\delta t) = v_x(t)\cos(\omega\delta t) + v_y(t)\sin(\omega\delta t) + \frac{1}{\omega}[-a_y^c(t)C(\omega\delta t) + a_x^c\sin(\omega\delta t)] + \frac{1}{\omega^2}\left[-\frac{a_x^c(t+\delta t) - a_x^c(t)}{\delta t}C(\omega\delta t) - \frac{a_y^c(t+\delta t) - a_y^c(t)}{\delta t}S(\omega\delta t)\right] + O((\delta t)^3)$$

$$v_y(t+\delta t) = \text{like } v_x(t+\delta t), \quad \text{exchange } x \leftrightarrow y, \quad \omega \leftrightarrow -\omega$$

$$\mathrm{v}_z(t+\delta t) = v_z(t) + \frac{1}{2}\delta t[a_z^c(t) + a_z^c(t+\delta t)] + O((\delta t)^3) \tag{20}$$

Since MD follows the trajectory of each particle, imposing the magnetic field into the equation of motion leads to the choice of a time step δt that is small enough to account for sufficient number of steps per Larmor oscillation in order to follow the motion of the particle correctly. Briefly stated, this explicit second-order accurate algorithm is efficient, permits local time-stepping and thus enlarges the domain of MD applications.

3. Numerical experiments

Two different polyethylene chains were generated. The chemical unrelaxed structures of the two different polyethylene chains-utilized in this investigation are shown in figure 1. The first chain was generated randomly through Monte Carlo algorithm and contains 902 atoms (600 H and 302 C). The other chain was designed in the shape of a helix with a diameter of (2.07 nm) and contains 388 atoms (259 H and 129 C).

The atomic force field used is the optimized potentials for liquid simulations-all atoms (OPLSAA) consists of harmonic bond-stretching and angle-bending terms, a Fourier series for torsional energetics and Coulomb and Lennard–Jones terms for the non-bonded interactions [17]:

$$E_{\text{bond}} = \sum_i k_{b,i}(r_i - r_{o,i})^2 \tag{21}$$

$$E_{\text{angle}} = \sum_i k_{\vartheta,i}(\vartheta_i - \vartheta_{o,i})^2 \tag{22}$$

$$E_{\text{torsion}} = \sum_i \left[\frac{1}{2}V_{1,i}(1+\cos\varphi_i) + \frac{1}{2}V_{2,i}(1-\cos 2\varphi_i) + \frac{1}{2}V_{3,i}(1+\cos 3\varphi_i)\right] \tag{23}$$

$$E_{\text{non-bonded}} = \sum_i\sum_{j>i}\left\{\frac{q_iq_je^2}{r_{ij}} + 4\varepsilon_{ij}\left[\left(\frac{\sigma_{ij}}{r_{ij}}\right)^{12} - \left(\frac{\sigma_{ij}}{r_{ij}}\right)^{6}\right]\right\} \tag{24}$$

Here, the parameters are the force constants k, the r_o and ϑ reference values, the Fourier coefficients V, the partial atomic charges q and the Lennard–Jones radii and

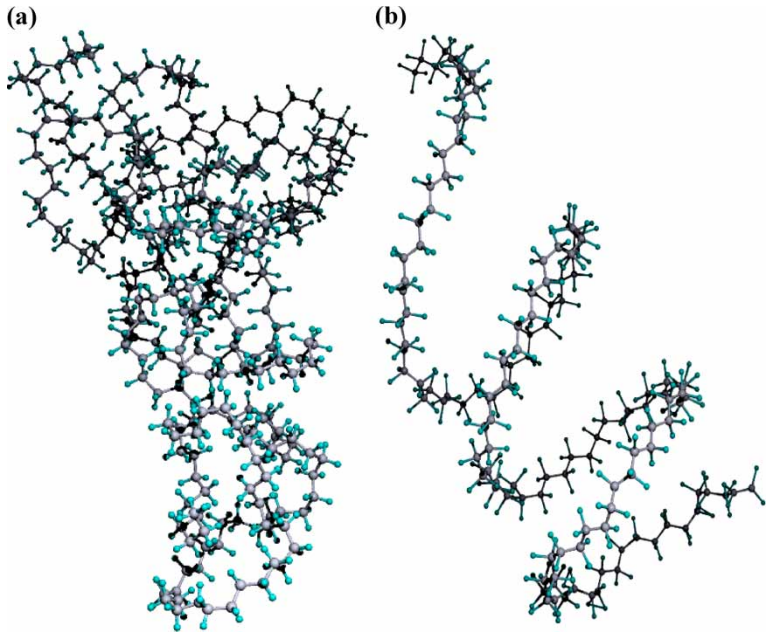

Figure 1. Unrelaxed configurations of (a) heavily folded polyethylene chain of 902 atoms, (b) helical polyethylene chain with 388 atoms.

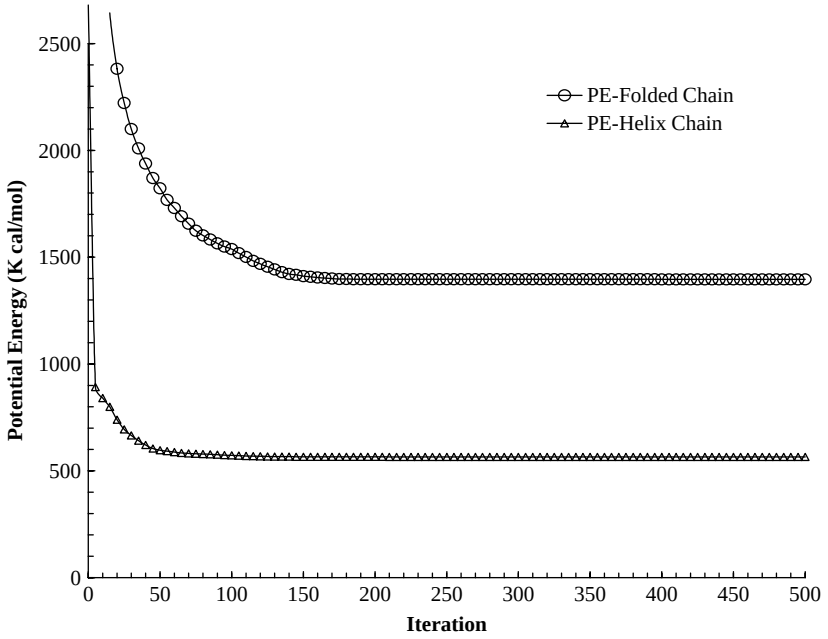

Figure 2. Minimum potential energy configuration for the individual polyethylene chains; minimization based on truncated Newton algorithm with rms 0.0001 Kcal/mol Å convergence.

well-depths, σ and ε. The non-bonded interactions are evaluated intermolecularly and for intramolecular atom pairs separated by three or more bonds. OPLSAA was parameterized, tested and validated for hydrocarbons [18–20].

All of the MD simulations were performed within the framework of the NPT (isothermal–isobaric) statistical ensemble for a periodic system [21], which is characterized, by a fixed number of atoms N, constant pressure P and constant temperature T. The NPT ensemble is an attractive choice. First, it allows the MD simulation for systems with relatively small number of particles (less than 1000 atom) [22] by calculating the trajectories in various ways. Second, the NPT ensemble simulates the effect of surrounding particles without creating undesirable surfaces. Third, this method simulates both the forces that drive the system to equilibrium at a given temperature and pressure and the forces that cause the energy and volume of the system to fluctuate about their equilibrium values [22]. Nose–Hoover extended system thermostat [23] was used for the temperature control and the Berendsen [24] barostat was used to maintain a constant desired pressure in the periodic box.

We started by equilibrating the individual systems of polyethylene. First, we employed a truncated Newton minimization method [25] in order to relax the initial configurations of the polyethylene chains to their local potential energy minimum. The initial dimensions of the boundary box for the folded polyethylene chain are $8.63 \times 3.64 \times 2.27$ nm and for the helical chain is $4.33 \times 1.88 \times 2.36$. The polyethylene cell is relaxed through the minimization of the potential energy to a convergence criterion where the rms atom force cutoff of the energy is 0.001 Kcal/mol Å. The final dimensions of the relaxed unfolded polyethylene cell are $5.0 \times 2.0 \times 2.94$ nm and for the helix chain $4.05 \times 1.78 \times 2.18$ nm, respectively.

4. Results and discussion

On achieving the state of minimum potential energy the relaxed potential energies of the polyethylene systems are shown in figure 2. After the potential energy of polyethylene reaches an equilibrium state we conducted MD simulations that employs a magnetic field of

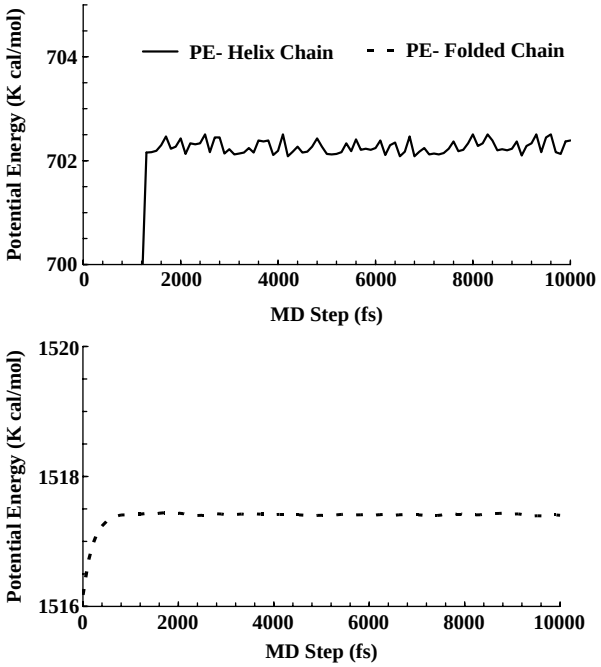

Figure 3. Potential energy evolution for polyethylene chains under 25 T magnetic field during 10 ps of MD simulation using NPT ensemble.

25 T (figure 3) directed along the z-axis direction. The simulations were carried out using TINKER™ software [26] by incorporating the modified velocity Verlet algorithm (equations (14) and (20)). Periodic boundary conditions were imposed precluding thus the effects of boundaries/walls. The integration time step was 1.0 femto second and the cutoff distance for the 12–6 Lennard–Jones potential was set to 1.05 nm. It is reasonable to assume equilibrium if the variation in the potential energy is in the range 0.0001–0.001 as discussed by Leach [21] (pp. 359). Following this criterion, equilibrium was achieved within 10 ps as shown in figure 4. The potential energy of the chain that was heavily folded increased by 12.3% compared to the relaxed potential energy without the magnetic field effect, while the helical chain gained 24.2% increase in its energy compared to the minimized relaxed configuration.

The extra potential energy gained through the magnetic annealing of the chains facilitated the reorientation of the polyethylene chains toward the direction of the magnetic.

The trajectory of the helical polyethylene chain with the 25 T magnetic field effect is shown at different instants in figure 4. The effect of the magnetic field manifests itself in the structural change at the chain level of the polyethylene chain. It is apparent that the helical polyethylene chain has completely unfolded within 2.5 ps into a linear form with a noticeable orientation parallel to the z-axis (figure 4), which is the direction of the external magnetic field. The chain was completely stretched toward the magnetic field at 7.5 ps and it maintained the alignment in the direction of the field after then a shown in figure 5.

The same reorientation behavior was observed for the heavily folded chain with more monomers. However complete unfolding occurred around 5 ps and full alignment was achieved in between 9 and 10 ps. The extra time needed to align this chain is mainly due to the fact it has more monomers and it is less organized compared to the helical chain.

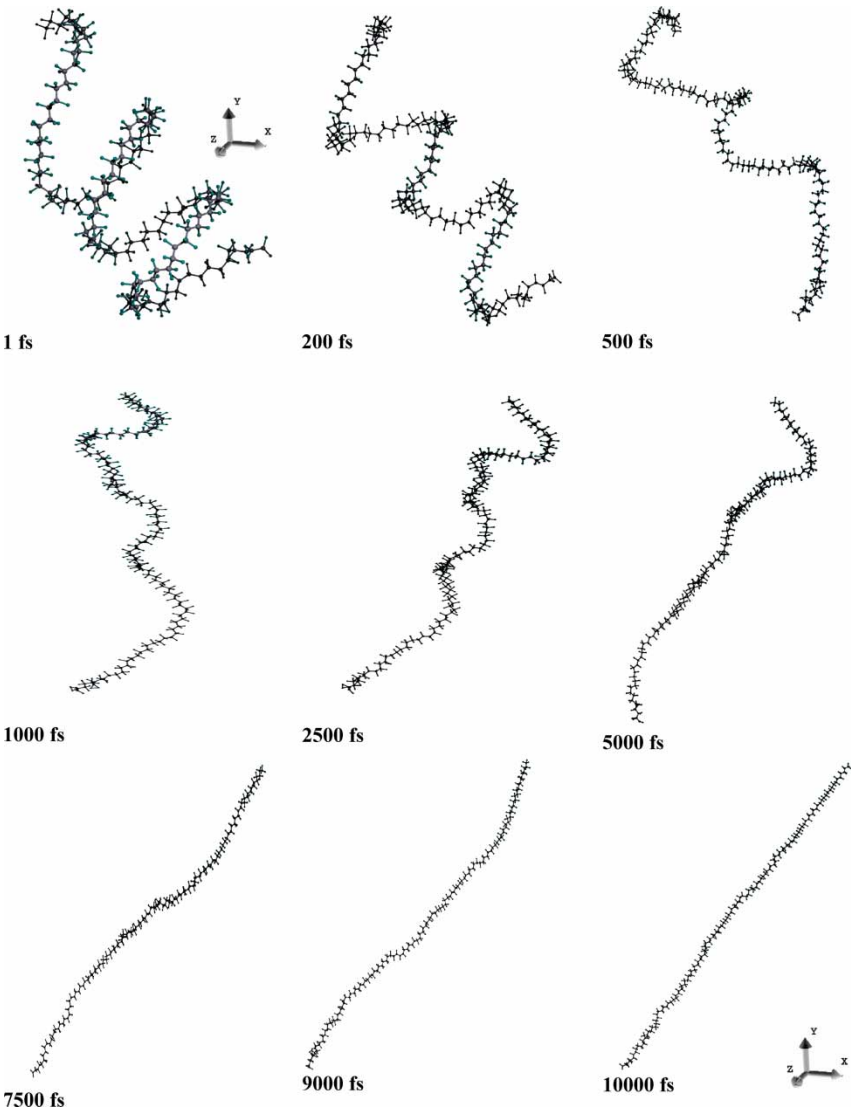

Figure 4. Instantaneous trajectory for the helical polyethylene chain at different time steps between 0 and 10 ps. Modified velocity form of Verlet algorithm utilizing a 25 T magnetic field along the z-axis was used to integrate the equation of motion. NPT ensemble was utilized through all the MD simulations.

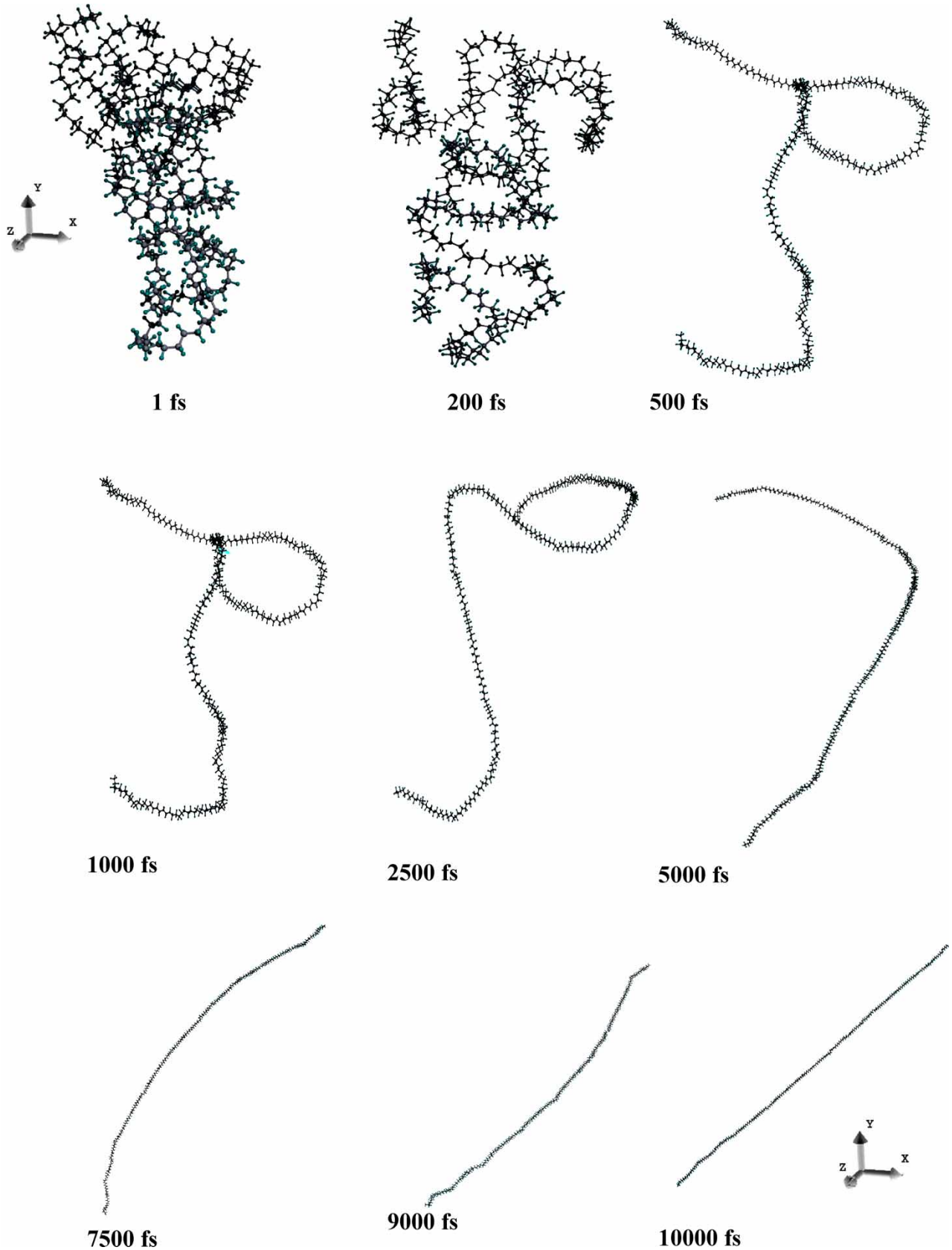

Figure 5. Instantaneous trajectory for the folded polyethylene at different time steps between 0 and 10 ps. Modified velocity form of Verlet algorithm utilizing a 25 T magnetic field along the z-axis was used to integrate the equation of motion. NPT ensemble was utilized through all the MD simulations.

The alignment of polyethylene under magnetic fields was found to depend on the initial configuration and the number of atoms in the chain. A chain with more order (helical) achieve alignment at relatively faster rate than a longer heavily folded chain.

5. Concluding remarks

The MD simulation results show that the magnetic field facilitates the unfolding of the flexible polyethylene chains and their reorientation in its direction. Magnetic processing of polyethylene was found to increase the potential energy of the system. MD simulations, based on the variant of the velocity Verlet algorithm, modified to incorporate strong static homogeneous external magnetic fields, are viable tool to study in a fast and inexpensive fashion the internal evolution of polymeric systems under the influence of strong magnetic fields.

References

[1] A. Horsch, Z.L. Zhang, S.C. Glotzer. Self-assembly of polymer-tethered nanorods. *Phys. Rev. Lett.*, **95**(056105) (2005).
[2] P.C.M. Christianen, I.O. Shklyarevskiy, M.I. Boamfa, J.C. Maan. Alignment of molecular materials in high magnetic fields. *Physica B.*, **346–347**, 255 (2004).
[3] D.S. Li, H. Garmestani, R.G. Alamo, S.R. Kalidindi. The role of crystallinity in the crystallographic texture evolution of polyethylenes during tensile deformation. *Polymer*, **44**, 5355 (2003).
[4] A. Shiota, C.K. Ober. Orientation of liquid crystalline epoxies under ac electric fields. *Macromolecules*, **30**, 4278 (1997).
[5] M.S. Al-Haik, H. Garmestani, D.S. Li, M.Y. Hussaini, S.S. Sablin, R. Tannenbaum, K. Dahmen. Mechanical properties of magnetically oriented epoxy. *J. Polym. Sci. B: Pol. Phys.*, **42**, 1586 (2004).
[6] B.C. Benicewicz, M.E. Smith, J.D. Earls, R.D. Priester, E.P. Douglas, *et al*. Magnetic field orientation of liquid crystalline epoxy thermosets. *Macromolecules*, **31**, 4730 (1998).
[7] T. Kimura, T. Kawi, Y. Sakamot. Magnetic orientation of poly (ethylene terephthalate). *Polymer*, **41**, 809 (2000).
[8] S. Kossikhina, T. Kimura, E. Ito, M. Kawahara. Structures and tensile properties of a magnetically and mechanically oriented liquid crystalline copolyester, Xydar. *Polym. Eng. Sci.*, **37**, 396 (1997).
[9] A. Anwer, A.H. Windle. Magnetic orientation and microstructure of main-chain thermotropic copolyesters. *Polymer*, **34**, 3347 (1993).
[10] T. Kimura. Study on the effect of magnetic fields on polymeric materials and its application. *Polym. J.*, **35**, 823 (2003).
[11] F. Ebert, T. Thurn-Albrecht. Controlling the orientation of semicrystalline polymers by crystallization in magnetic fields. *Macromolecules*, **36**, 8685 (2003).
[12] E.S. Choi, J.S. Brooks, D.L. Eaton, M.S. Al-Haik, M.Y. Hussaini, H. Garmestani, D. Li, K. Dahmen. Enhancement of thermal and electrical properties of carbon nanotube polymer composites by magnetic field processing. *J. Appl. Phys.*, **94**, 6034 (2003).
[13] H. Garmestani, M.S. Al-Haik, K. Dahmen, R. Tannenbaum, *et al*. Polymer-mediated alignment of carbon nanotubes under high magnetic fields. *Adv. Mater.*, **15**, 1918 (2003).
[14] T.A. Weber, N.D. Annan. Molecular-dynamics of small alkanes in an external force-field. *Mol. Phys.*, **46**, 193 (1982).
[15] P. Tian, B. Bedrov, G.D. Smith, *et al*. A molecular-dynamics simulation study of the switching dynamics of a nematic liquid crystal under an applied electrical field. *J. Chem. Phys.*, **117**, 9452 (2002).
[16] Q. Spreiter, M. Walter. Classical molecular dynamics simulation with the velocity Verlet algorithm at strong external magnetic fields. *J. Comput. Phys.*, **152**, 102 (1999).
[17] R.C. Rizzo, W.L. Jorgensen. O.P.L.S. all-atom model for amines: Resolution of the amine hydration problem. *J. Am. Chem. Soc.*, **121**, 4827 (1999).
[18] L. Lue, D. Blankschtein. Liquid-state theory of hydrocarbon water-systems—application to methane, ethane, and propane. *J. Phys. Chem.*, **96**, 8582 (1992).
[19] W.L. Jorgensen, D.S. Maxwell, J. Tirado-Rives. Development and testing of the OPLS all-atom force field on conformational energetics and properties of organic liquids. *J. Am. Chem. Soc.*, **117**, 11225 (1996).
[20] G. Kaminski, W.L. Jorgensen. Performance of the AMBER94, MMFF94, and OPLS-AA force fields for modeling organic liquids. *J. Phys. Chem.*, **100**, 18010 (1996).
[21] S. Toxvaerd. Molecular-dynamics at constant temperature and pressure. *Phys. Rev. E.*, **47**, 343 (1993).
[22] H.C. Andersen. Molecular dynamics simulations at constant pressure and/or temperature. *J. Chem. Phys.*, **72**, 2384 (1980).
[23] G.J. Martyana, M.E. Tuckerman, D.J. Tobias, M.L. Klein. Explicit reversible integrators for extended systems dynamics. *Mol. Phys.*, **87**, 1117 (1996).
[24] H.J.C. Berendsen, J.P.M. Postma, W.F. van Gunsteren, *et al*. Molecular-dynamics with coupling to an external bath. *J. Chem. Phys.*, **81**, 3684 (1984).
[25] M.S. Al-Haik, H. Garmestani, I.M. Navon. Truncated Newton training algorithm for neurocomputational viscoplastic model. *Comput. Methods Appl. Mech. Eng.*, **192**, 2249 (2003).
[26] M.J. Dudek, J.W. Ponder. Accurate modeling of the intramolecular electrostatic energy of protein. *Comput. Chem.*, **6**, 791 (1995).